



SPE-170819-MS

Investigating Aperture-Based Stress-Dependent Permeability and Capillary Pressure in Rock Fractures

Da Huo and Boxiao Li, SPE; Sally M. Benson, Stanford University

Copyright 2014, Society of Petroleum Engineers

This paper was prepared for presentation at the SPE Annual Technical Conference and Exhibition held in Amsterdam, The Netherlands, 27–29 October 2014.

This paper was selected for presentation by an SPE program committee following review of information contained in an abstract submitted by the author(s). Contents of the paper have not been reviewed by the Society of Petroleum Engineers and are subject to correction by the author(s). The material does not necessarily reflect any position of the Society of Petroleum Engineers, its officers, or members. Electronic reproduction, distribution, or storage of any part of this paper without the written consent of the Society of Petroleum Engineers is prohibited. Permission to reproduce in print is restricted to an abstract of not more than 300 words; illustrations may not be copied. The abstract must contain conspicuous acknowledgment of SPE copyright.

Abstract

Understanding multi-phase fluid flow behavior in fractured porous media is crucial for developing fractured hydrocarbon reservoirs, implementing hydraulic fracturing, and predicting potential leakage in gas and CO₂ storage. The goal of this research is to investigate stress-dependent permeability and capillary pressure in rock fractures. Laboratory measurements of fracture aperture distributions have been made using CT scanning under various conditions of effective stress. By applying the stress-dependent aperture data, numerical simulation is employed to model the change of permeability and capillary pressure in the rock fracture as a function of the effective stress.

The stress-dependent aperture distribution data demonstrates that increasing stress results in two effects: (1); the mean aperture will decrease; (2); the variance of aperture distribution will increase. Experimental results show that permeability will drop by 73% when effective stress increases from 0.34MPa to 22.06MPa. As the variance of aperture distribution increases with stress, the plateau area of the capillary pressure curve tends to grow steeper, indicating that capillary behavior changes from more fracture-like to more porous media-like. The impacts of mean and variance of aperture distributions on permeability and capillary pressure are separately analyzed. The mean aperture decrease will reduce permeability and increase entry pressure. The variance increase will reduce permeability, the pore size distribution index and entry pressure. By analyzing the stress-dependent mean and variance of aperture distributions, this paper provides a more straightforward way for estimating stress-dependent permeability and capillary pressure in rock fractures.

Introduction

Understanding fluid flow behavior in fractures is essential for petroleum production, especially for highly fracture-dominated systems, such as shale gas/oil production (Wang et al., 2009; Cho et al., 2012);, enhanced oil recovery (Babadagli, 2003; Wan et al., 2013);, and predicting potential natural gas/CO₂ leakage (Pruess, 2008; Huo and Gong, 2010);. Since fractures generally have crack-like shape and thus are more susceptible to stress, the fluid behavior in fractures will be stress-dependent. Stress-dependent permeability, and capillary pressure in fractures will have significant influence in fluid injection/production (Wan et al., 2013; Pinzon et al., 2000; Abass et al., 2009);.

Rock fractures are composed of variable fracture voids and thus they are highly heterogeneous. Fracture aperture distributions can be represented by gamma function distributions (Gentier, 1986);, truncated normal distributions (Walsh, 2008); or lognormal distributions (Tsang and Tsang, 1990);. All distributions demonstrate a right skewed aperture distribution with a long tail, demonstrating that smaller apertures outnumber larger apertures. Fracture voids tend to be more crack-like compared with oval or triangular shape of pores in porous media. Hence, they deform easily and have a higher degree of stress sensitivity (National Research Council, 1996);. Changes in either normal stress or shear stress can alter the aperture dimension and aperture distribution of a fracture (Brace, 1978; Esaki et al., 1998; Esaki et al., 1999);. In this paper, we focus on the impact of normal stress on aperture change. Increasing stress reduces both mechanical aperture (the arithmetic mean of the aperture field); and hydraulic aperture (the effective mean aperture of the fracture used in Cubic Law);. Depending on grain type and aperture distributions, aperture changes are heterogeneous. Results from Muralidharan et al. (2004); show that aperture distributions follow lognormal distributions under various stress conditions. Longer tail and more right skewed aperture distribution are observed with increasing stress (Walsh et al., 2008; Muralidharan et al. 2004);. Variances of aperture distribution either stay constant (Liu et al., 2013);, or decrease (Muralidharan et al., 2004); or increase (Walsh et al., 2008);.

Research on calculating fracture permeability has been undergoing for decades (Brace, 1978; Walsh, 1981; Zimmerman et al., 1992);. The most widely recognized model is the Cubic Law (Boussinesq, 1868); and Modified Cubic Law (Witherspoon, 1980);. The Modified Cubic Law is shown as:

$$q = -\frac{1}{f} \frac{e^3}{12\mu} \frac{dp}{dx} \quad (1)$$

where q is the flow rate per unit width of the fracture, e is the aperture between separated plate surfaces, $\frac{dp}{dx}$ is pressure gradient, μ is the fluid viscosity, and f is the friction factor to account for the roughness of fracture surfaces. Both models apply the fracture aperture as a constant parameter to calculate the permeability. In addition, the Modified Cubic Law introduces a friction factor to account for the roughness and tortuosity of the fracture surface. Conventionally, the fracture aperture is calculated as the mean of the fracture plane displacement. The friction factor accounts for all surface phenomena that impede fluid flow beyond that expected based on smooth parallel plates, including roughness and tortuosity (Murata and Saito, 2003);. Multiple realizations of friction factor include calculating the standard deviation of aperture distribution, considering effect of fracture surface contact area, and shapes of the obstructions (Renshaw, 1995; Walsh, 1981; Zimmerman, 1991);. The relative direction of fluid flow and the obstruction shape also affect the flow behavior and different relationships are developed between friction factor and shape of contact area (Patir and Cheng, 1978);.

Stress-dependent aperture distributions cause the permeability to be stress-dependent. At low to moderate effective stress, aperture changes can result in up to three orders of magnitude of conductivity loss at early stages of reservoir depletion (Abass et al., 2009);. In terms of the Modified Cubic Law, fracture aperture and friction factor are both subject to stress change (Huo and Benson, 2014);. Increasing stress will reduce the aperture and raise the friction factor. The friction factor change is due to the heterogeneity of aperture change, which creates a rougher and more tortuous path. Additionally, increasing compressive stress will result in more contacted asperities and thus more tortuous flow channels (Raven and Gale, 1985);. At low stresses, natural fracture openings diminish more rapidly than fracture closure. Due to the increase of fracture stiffness, at high stresses, aperture and tortuosity of those portions of the flow path that impede flow become virtually independent of stress (Cook et al., 1990; Pyrak-Nolte et al., 1990);.

By conceptualizing the fracture as a two-horizontal-plane system, the capillary pressure curve for fracture aperture has a very low entry pressure (calculated from interfacial tension and fracture aperture); and a very flat plateau region. Consequently, as soon as the nonwetting phase invades the fracture, the

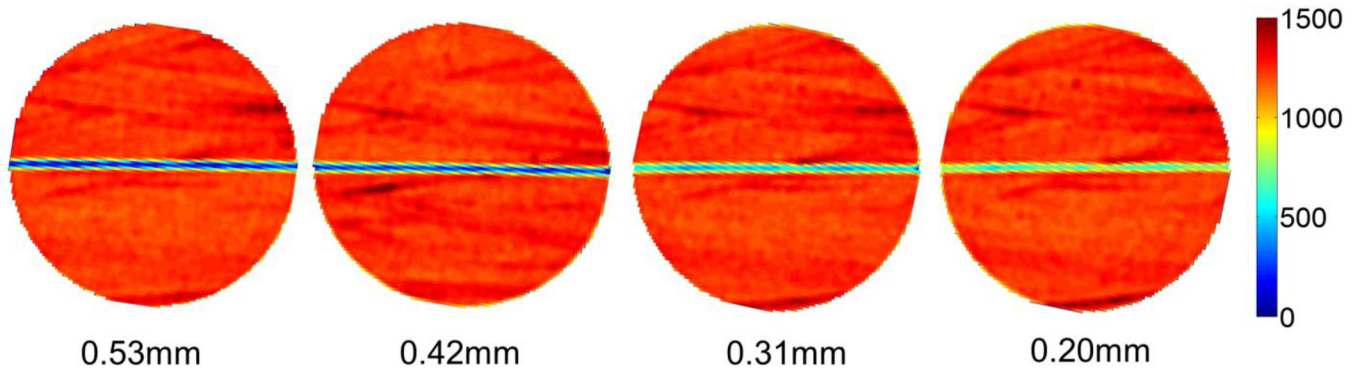


Figure 2—Calibration image of Berea sandstone with different spacers. Each image is the average of 20 scans. The colorbar represents the CT number.

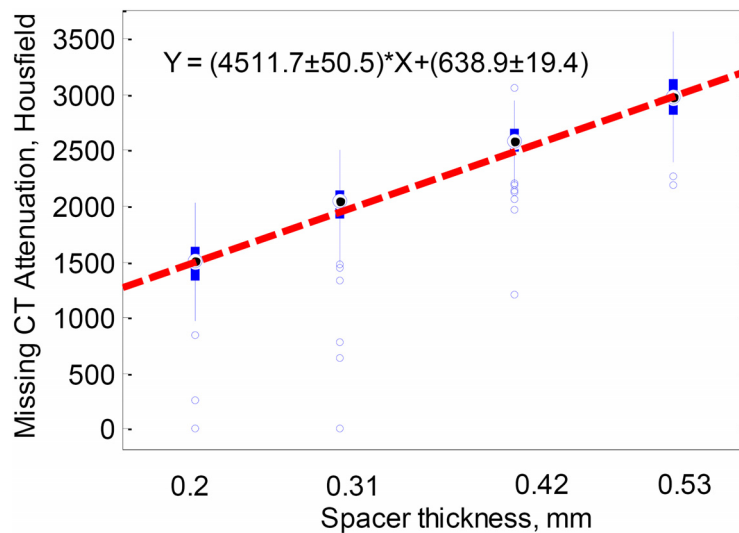


Figure 3—Calibration of missing CT attenuation and spacer thickness. The standard deviation of slope is also calculated. The thick blue lines show the 25% confidence interval while the thin blue line shows the 75% confidence interval. The circles above and below the thin blue lines are outliers. The dashed red line corresponds to fitting between missing CT attenuation and spacer thickness.

resolution X-Ray CT imaging; (2); stress-dependent capillary pressure curves are modeled using numerical simulations based on the realistic aperture field we obtain from the experiment; and (3); stress-dependent permeability and capillary pressure are analyzed from the perspective of mean and variance of aperture distribution.

Experimental setup

A Berea sandstone is saw-cut to create a fracture in the middle of the core. The sample is moderately homogeneous with little porosity variation. The fracture surface is very rough and has large aperture variations. The length of the sample is 8 cm and the radius is 5 cm. The porosity of the sample is 0.22. The rock sample is wrapped in a sleeve with one layer of heat-shrinkable Teflon, and a viton rubber sleeve, and then placed in an aluminum core holder. Water is injected around the sleeve to create the confining stress (Teledyne Isco, model 260D); Two high accuracy pressure transducers (Oil filled Digiquartz Intelligent Transmitter, model 9000–3K-101); are tapped into the core holder to measure pressure at the inlet and outlet of the core. Electric heaters maintain the temperature of the core. Pore pressure is kept constant as atmospheric pressure and temperature keeps constant at 50 °C. For permeability measurements, a dual-pump system is used to inject water into the core (Teledyne Isco, model 500D);. A pressure-regulating pump (Teledyne Isco, model 1000D); is connected to the outlet of

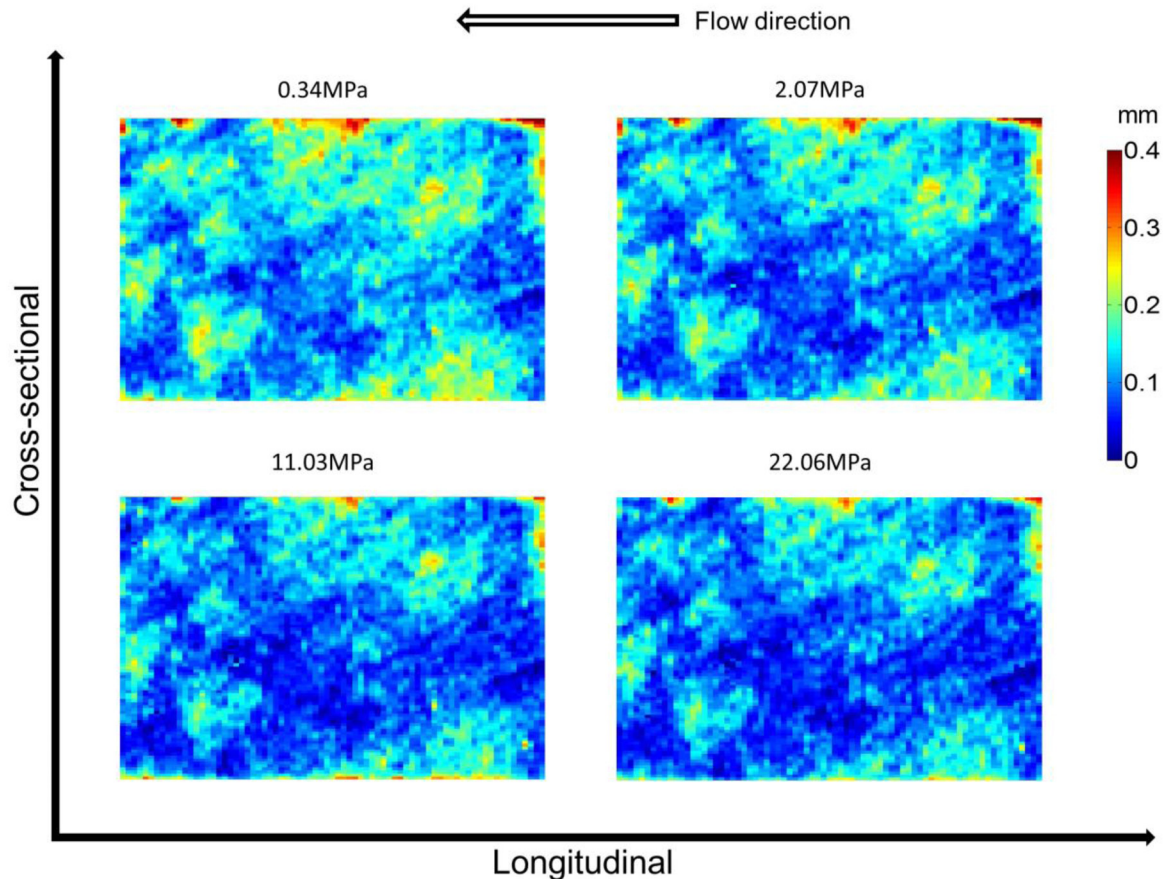


Figure 4—Aperture distribution at different stress levels. The effective stress is provided at the top of the images. The flow direction is applied in the experimental measurement.

the core through a recirculation pressure vessel to maintain 2.07MPa at the downstream end of the core throughout the experiment. The experimental setup is shown in Fig. 1.

Permeability is measured using the steady state method. Fluid is injected at three different rates while the pressure drop across the core is measured. Based on core size, fluid viscosity and slope of pressure drop and fluid injection rate, Darcy's law is used to calculate permeability. The intact core permeability is measured at different stress levels and been subtracted from the fractured core permeability. Permeability is calculated using a mean aperture of 0.1 mm.

The core holder is placed in a medical X-ray CT scanner (General Electric Hi-Speed CT/i X-ray computed tomography);. The following X-ray CT scanner parameters are applied: a voxel dimension of $0.5 \times 0.5 \times 1 \text{ mm}^3$, a tube current of 200 mA, an energy level of 120 keV and a display field of view of 25 cm. Five repeated scans are taken and averaged to reduce the uncertainty of the CT (Pini et al., 2012; Huo and Benson, 2014);.

Method for measuring fracture aperture using CT scanning

Fracture apertures are determined by the missing attenuation method based on calibration using spacers of known thickness (Johns et al., 1993; Keller, 1997; Van Geet and Swennen, 2001);. The missing CT attenuation (CT_{MA}); is defined as:

$$CT_{MA} = \sum_{i=1}^{N_{vox}} (CT_{mat} - CT_i) \quad (4)$$

where CT_{mat} represents the average CT value of rock matrix, CT_i represents the CT values of the

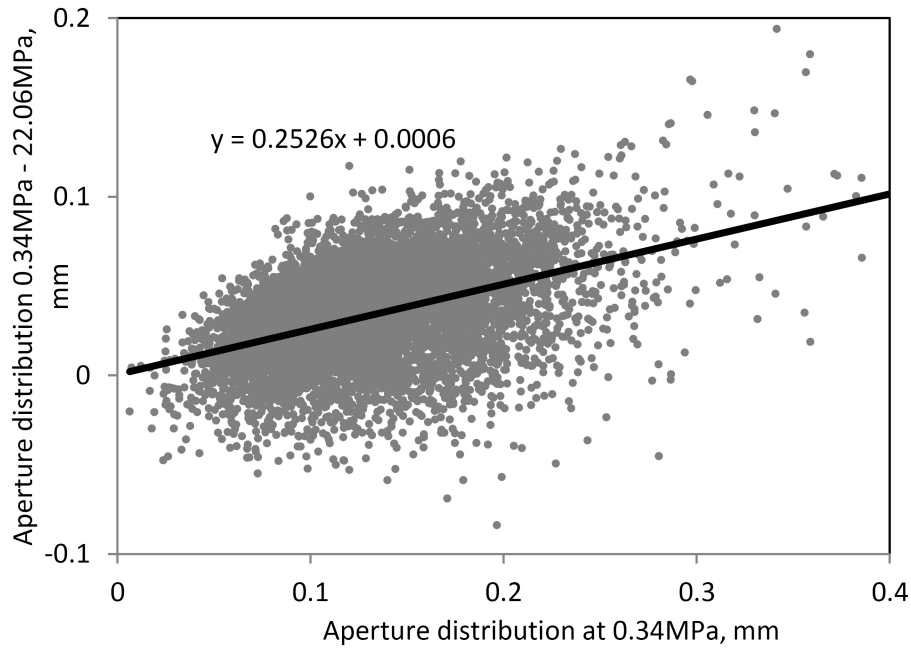


Figure 5—Aperture changes from 0.34MPa to 22.06MPa versus aperture distribution at 0.34MPa. The grey points show the aperture change versus aperture value at 0.34MPa. The black curve provides a linear regression.

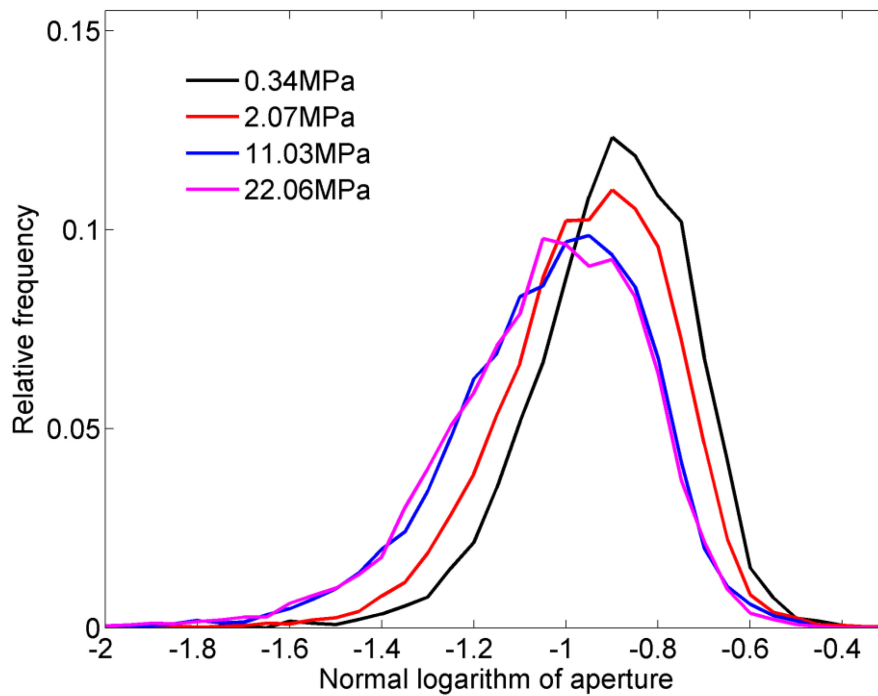


Figure 6—Comparison of relative frequency for normal logarithm of aperture at different stress levels. The aperture units are in millimeters.

transect across the trough and N_{vox} represents the voxel number of the line across the trough. The fracture aperture is related to the missing attenuation by:

$$e = \frac{CT_{MA}}{c} \quad (5)$$

Table 1—Comparison of statistical analysis of normal logarithm of aperture

Effective stress, MPa	Arithmetic mean of normal logarithm of aperture	Corresponding aperture, mm	Standard deviation of normal logarithm of aperture	Spatial correlation, horizontal direction, mm	Spatial correlation, vertical direction, mm
0.34	-0.9012	0.1255	0.1715	23.38	5.62
2.07	-0.9573	0.1103	0.1942	21.77	4.87
11.03	-1.0400	0.0912	0.2499	15.83	4.23
22.06	-1.0515	0.0888	0.2561	15.85	2.78

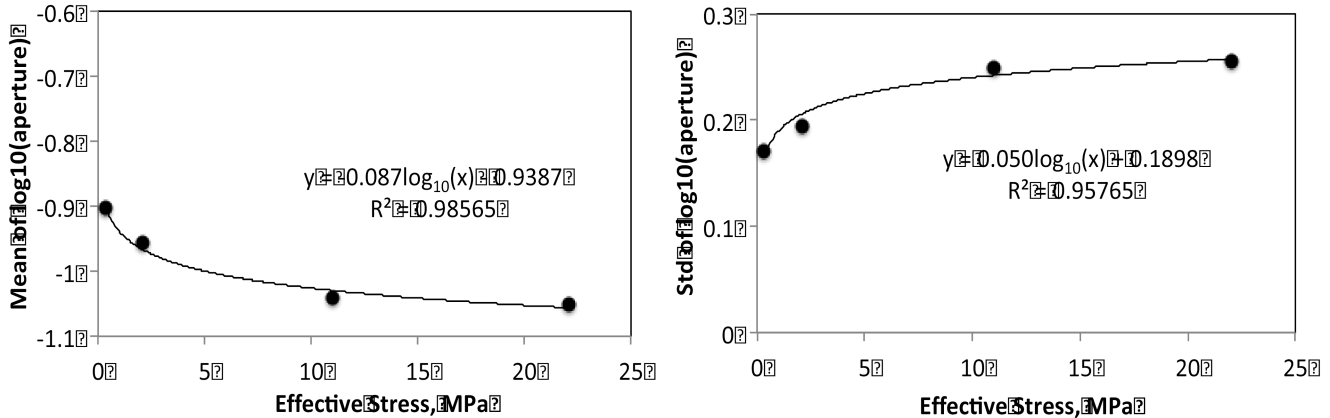


Figure 7—Stress-dependent mean and standard deviation (std); of normal logarithm of aperture distribution. Mean and standard deviation are fitted with effective stress using logarithm function.

where e is the fracture aperture and C is the calibration coefficient. In this experiment, calibration coefficients are determined using spacers of 0.20, 0.31, 0.42 and 0.53 mm between the two rock surfaces. After the sample has been placed into the core holder, a slight confining stress of 0.34MPa is added to flatten the spacer. For the calibration, twenty scans are taken to further increase the accuracy of CT scanning. The images of scans with different spacers are shown in Fig. 2. During the calibration, temperature is kept constant at 50 °C.

To calculate the missing attenuation due to the presence of a fracture; data cropping, classification, and identification of fracture features are needed (Karpyn, 2009);. The missing attenuation is calculated using Eq. 4. The calibration curve is shown in Fig. 3. Linear regression between missing attenuation and spacer thickness shows that the calibration coefficients are 4511.7 ± 50.5 . The regression line does not pass through the origin, suggesting that the missing attenuation caused by the roughness of the fracture creates an apparent aperture of 0.14 mm.

Experimental Data

Before the experiment, a cycle of stress from 0.34MPa to 11.03MPa is performed for setting the aperture asperities. Different effective stress levels, including 0.34MPa, 2.07MPa, 11.03MPa and 22.06MPa, are applied in a second cycle. The aperture distribution maps are calculated using Eq. 5 and shown in Fig. 4. Pockets of large and small apertures can be clearly observed, suggesting the aperture distribution is highly heterogeneous. With increasing stress, fracture apertures become smaller. The stress-dependent aperture changes are also heterogeneous. Larger apertures tend to have larger changes with stress increase (Fig. 5);.

Figure 6 shows a histogram of the logarithm of the aperture distributions. With increasing stress, the mean aperture decreases and the standard deviation increases (Table 1);. Both effects are expected to reduce permeability and alter the capillary pressure curve. The spatial correlations (calculated using the

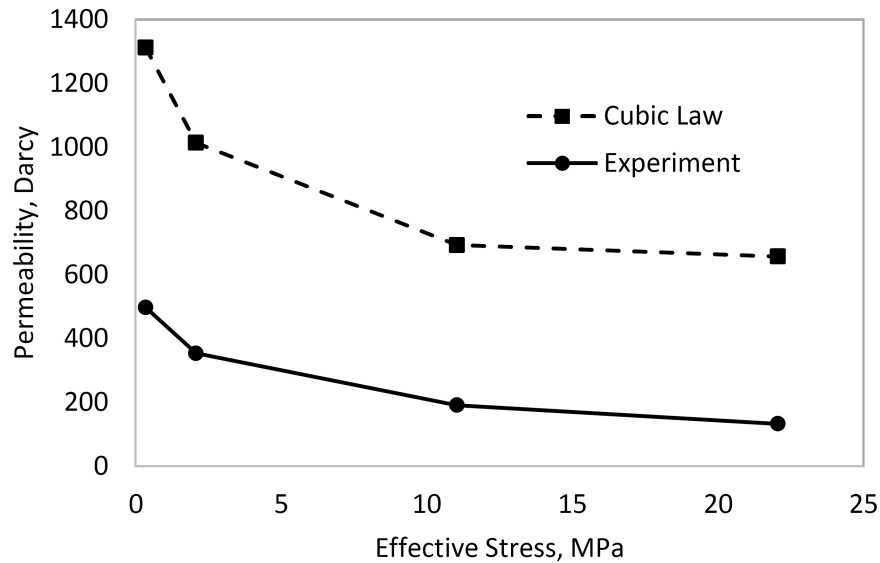


Figure 8—Stress-dependent permeability calculated using Cubic Law and experimental measurement.

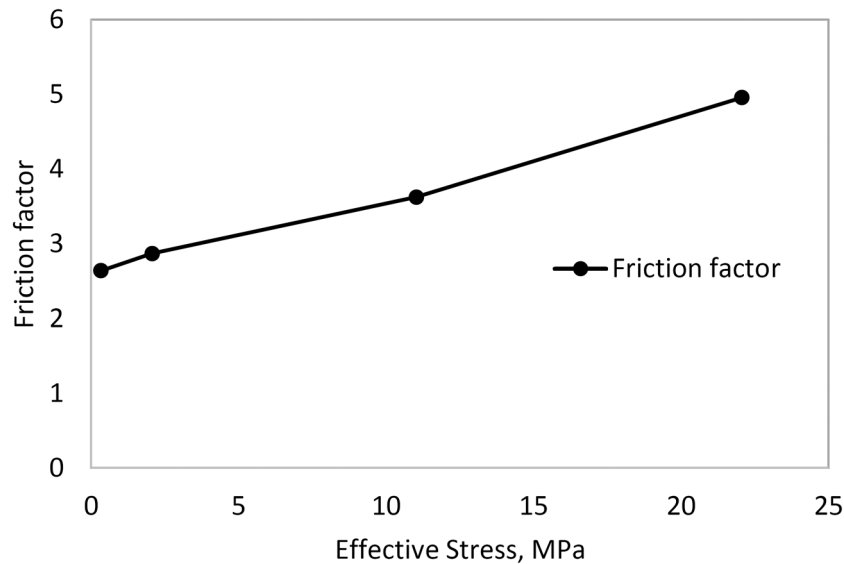


Figure 9—Stress-dependent friction factor. The friction factor is calculated using Eq. 1.

range of spherical variogram model); in both horizontal and vertical direction decrease with increasing stress.

In Fig. 7, the changes of mean and standard deviation of normal logarithm of aperture distribution are plotted with corresponding stress levels. Logarithm fitting is applied between mean/standard deviation and effective stress. This provides an approach to estimate the aperture distribution under different stress levels.

Results and discussion

Stress-dependent permeability

To calculate the stress-dependent permeability, another cycle of stress is conducted to measure the permeability using water. Before applying stress, CO₂ flooding and water flooding are performed

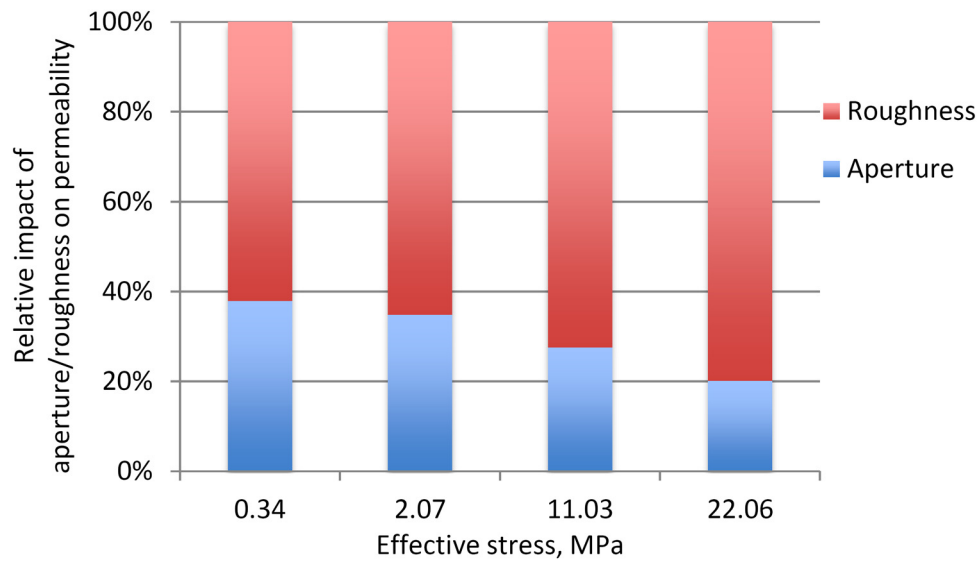


Figure 10—Relative impact of aperture and roughness on permeability. The relative impact of aperture is calculated by dividing experimentally measured permeability from permeability calculated using Cubic Law.

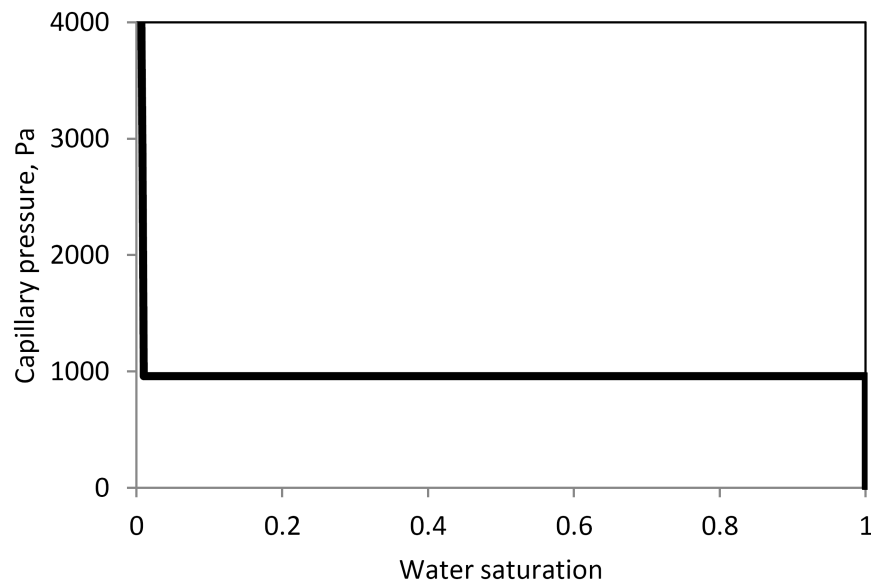


Figure 11—Capillary pressure curve for a single grid with 0.15 mm aperture.

successively to ensure no air is present in the sample. The comparison between the Cubic Law and experimental measurements shows that the permeability calculated by Cubic Law is 2.6 to 4.9 times larger than measured permeability (Fig. 8);. This demonstrates that the mean aperture change cannot fully describe the permeability drop, which is due to the increasing friction factor (Fig. 9);. From the perspective of Modified Cubic Law (Witherspoon, 1980);, the decreasing mean aperture will reduce the aperture e , and the increasing aperture variance will enhance the friction factor. Both effects will cause the fracture permeability to decrease. Roughness has a larger impact on permeability at higher stress (Fig. 10);.

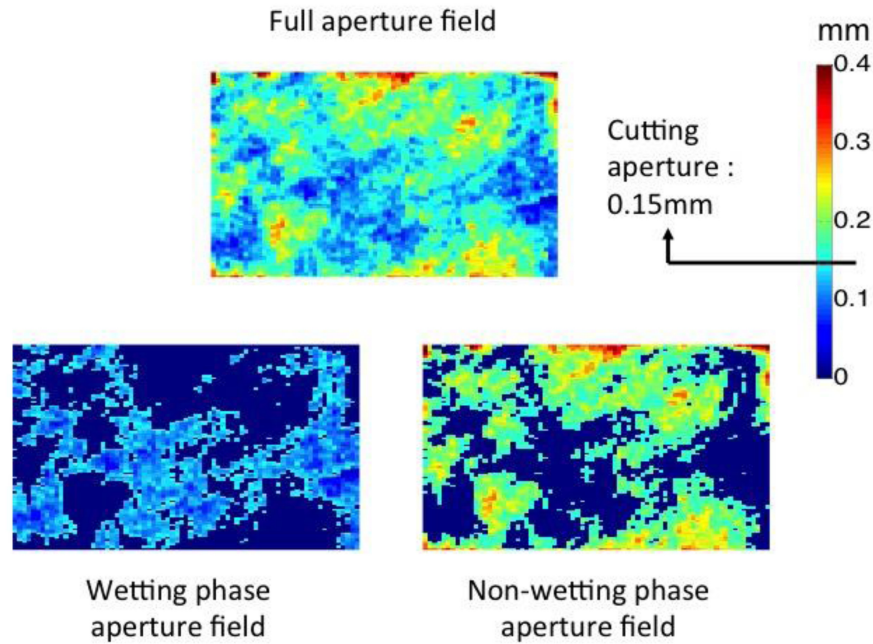


Figure 12—Fluid distribution on the fracture at a capillary pressure of 960 Pa. The upper field shows the full aperture field, the lower left field is the nonwetting-phase-filled apertures and the lower right field is the wetting-phase-filled apertures. The critical aperture for this capillary pressure is 0.15 mm.

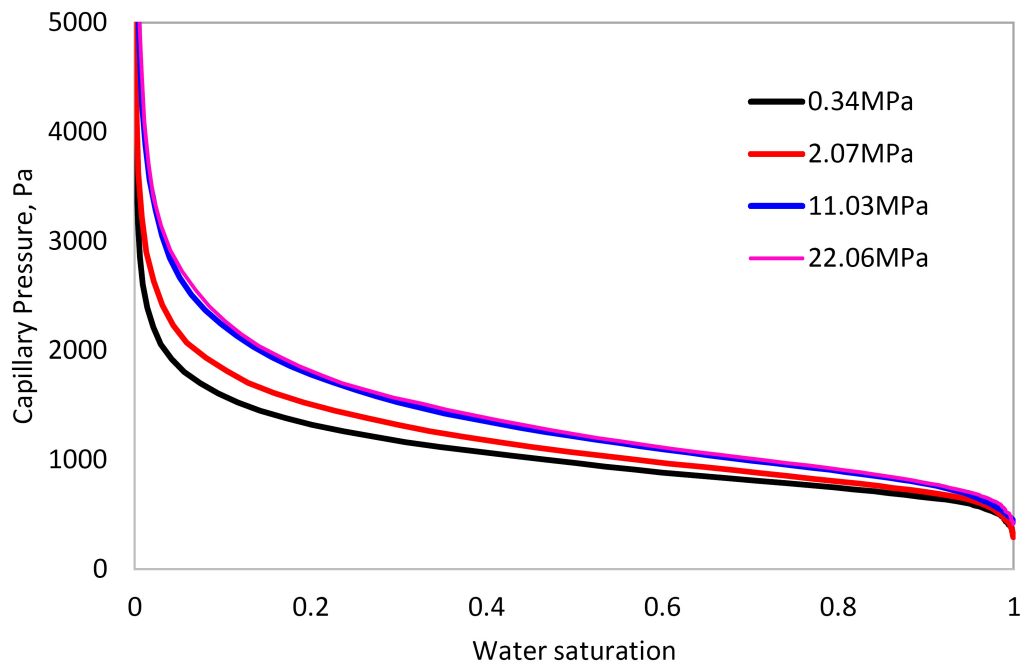


Figure 13—Stress-dependent capillary pressure for the rock fracture.

Stress-dependent capillary pressure

The capillary pressure curve for a single aperture fracture is calculated using Young-Laplace equation:

$$P_c = \frac{2\gamma\cos\theta}{e} \quad (6)$$

where P_c is the capillary pressure, γ is interfacial tension, θ is the contact angle, and e is the fracture aperture (Yang et al., 2013). Here we choose $\gamma = 72$ mN/m, $\theta = 0^\circ$, and P_c varies with fracture aperture.

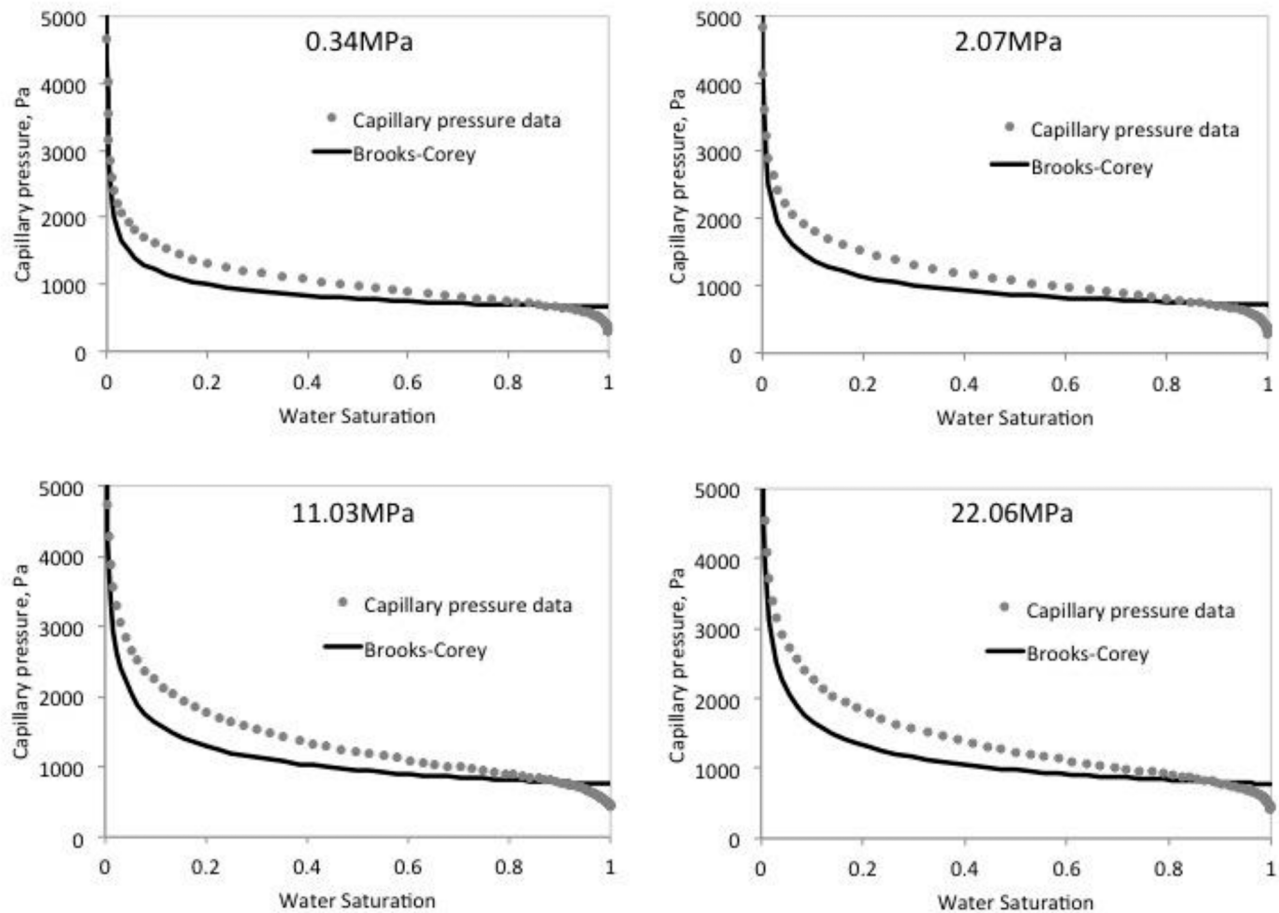


Figure 14—Brooks-Corey fitting of the capillary pressure data at different effective stress levels.

We assume each aperture has its own capillary pressure curve, which acts like a parallel plate, shown in Fig. 11.

The pore occupancy model is applied to calculate the capillary pressure curve for the fracture (Pruess and Tsang, 1990; Liu et al., 2013);. A critical aperture is determined based on the capillary pressure using Eq. 6. Apertures below the critical aperture are fully water saturated, while apertures above the cutting aperture are fully air saturated (Lenormand et al., 1983);. Average water saturation in the fracture is calculated using the fracture volume filled with water divided by the total fracture volume. The capillary pressure curve is obtained by relating the capillary pressure and the corresponding saturation. An example of the pore volume occupancy for a particular capillary pressure is shown in Fig. 12.

Applying the pore occupancy model, the stress-dependent capillary pressure curves are shown in Fig. 13. Since the variance of aperture distribution increases, the plateau area of the capillary pressure curve grows steeper with stress. This means that the capillary behavior changes from more fracture-like to more porous media-like. The entry pressure will also increase with increasing stress.

The capillary curves are fitted to the Brooks-Corey function, shown in Fig. 14 and Table 2. From the Brooks-Corey model, increasing stress level will cause the pore size distribution index to decrease and entry pressure to increase. The pore size distribution change agrees with the simulation results from Yang

Table 2—Brooks-Corey fitting for the capillary curve in Fig. 13

Effective stress, MPa	λ	Pe , Pa
0.34	3.83	657.22
2.07	3.44	710.82
11.03	3.00	756.50
22.06	2.99	775.95

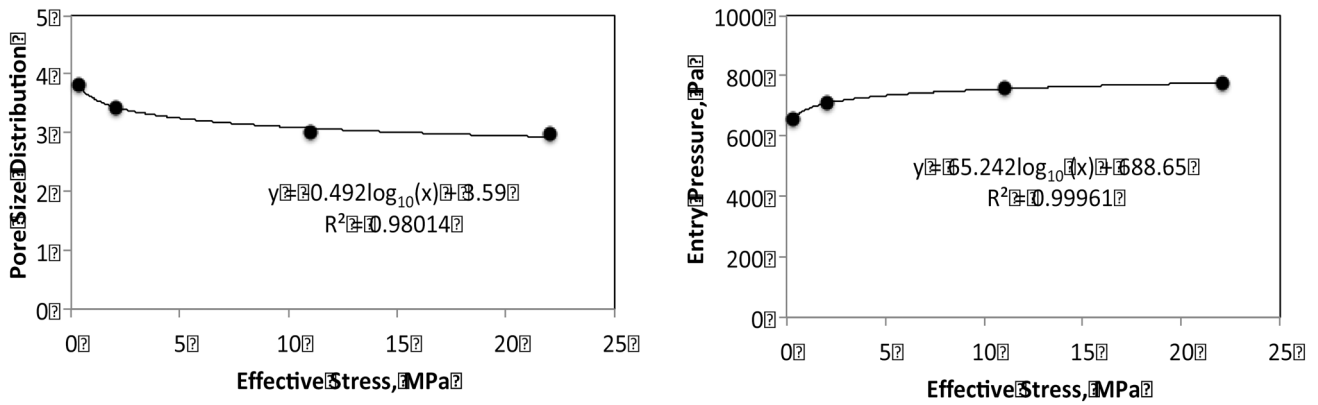


Figure 15—Pore size distribution index and entry pressure change with effective stress. The pore size distribution index and the entry pressure are both fitted with effective stress using logarithm function.

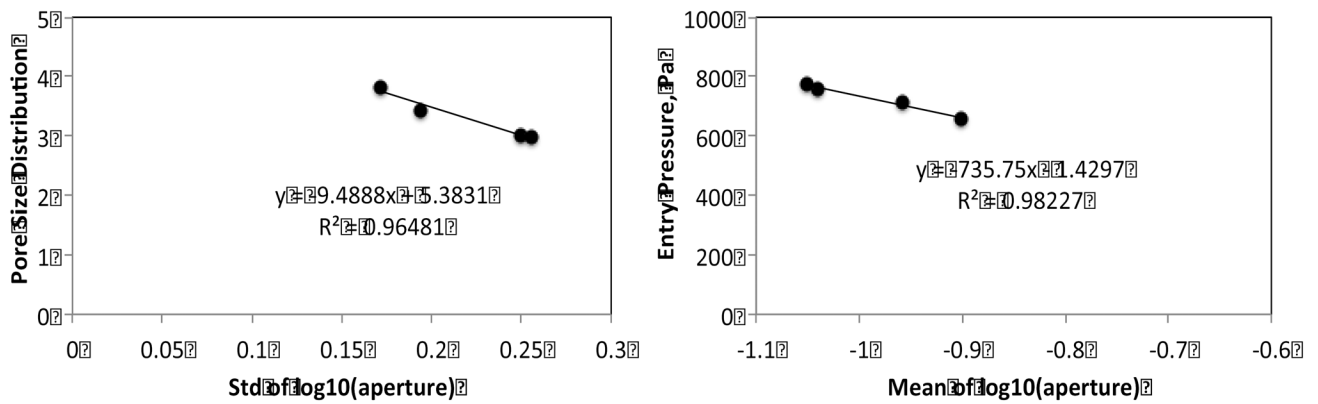


Figure 16—The impact of mean and standard deviation of aperture distribution on pore size distribution index and entry pressure.

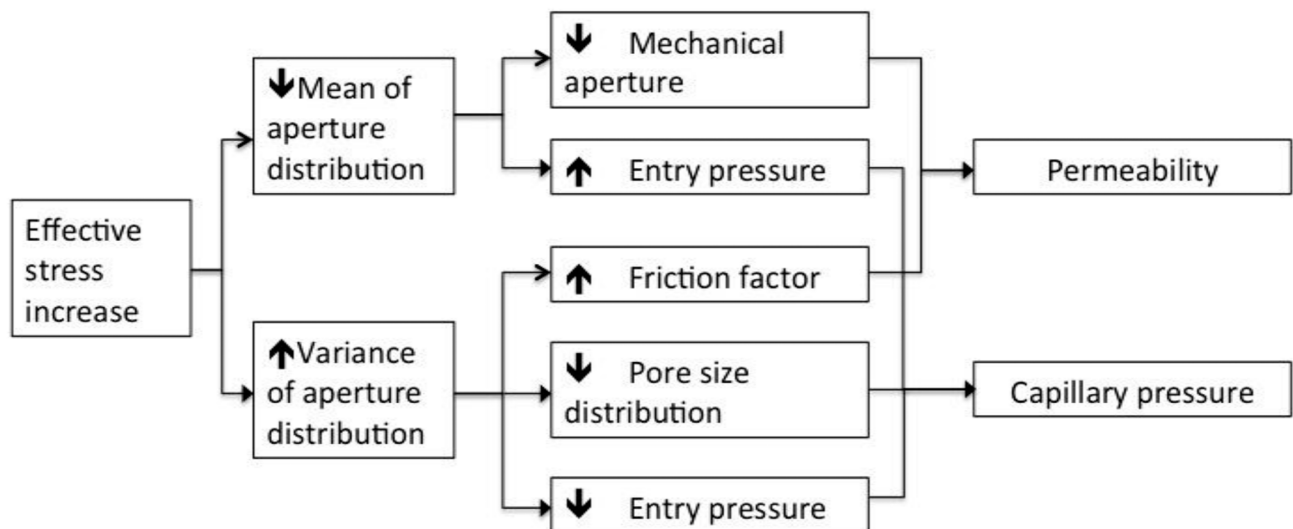


Figure 17—Relationship of effective stress with permeability and capillary pressure for rock fractures.

et al. (2013);, and is due to the increasing variance of aperture distribution. The entry pressure increase is caused by aperture decrease (Liu et al., 2013);. From Yang et al. (2013);, the increasing pore size distribution will also reduce the entry pressure. For these data, the impact of change in mean aperture is larger than the change in variance, thus the entry pressure will increase with stress.

Fig. 15 shows the pore size distribution index and entry pressure with respect to effective stress. Logarithm regressions between pore size distribution/entry pressure and effective stress demonstrate the relationships can be well presented using a logarithm function. From Fig. 16, the entry pressure has a negative correlation with the logarithm of the mean aperture, and increasing variance of aperture distribution will reduce the pore size distribution index.

Based on these data and previous research (Yang et al., 2013; Liu et al., 2013; Walsh, 1981; Walsh et al., 2008; Muralidharan et al. 2004);, we propose a two-component relationship for stress-dependent permeability and capillary pressure in rock fractures (Fig. 17);. Changes on both the mean aperture and variance of the aperture distribution cause the permeability decreases with increasing stress. For stress-dependent capillary pressure, the capillary curve plateau will grow steeper with increasing stress and the entry pressure will depend on relative changes of the mean and variance of aperture distribution.

Conclusions

In this paper, we measure the stress-dependent aperture distribution of a fractured Berea sandstone using the X-ray CT scanning technique. A pore occupancy model is used to determine the stress-dependent capillary pressure of the fracture. Based on the results and discussions, we have following conclusions:

1. The fracture aperture distribution is heterogeneous and stress-dependent. Larger apertures will have larger changes with stress.
2. Increasing stress will reduce the fracture apertures. Statistically it has two impacts: (1); the mean aperture will reduce; (2); the variance of aperture distribution will increase, thus the fracture will become smaller and more heterogeneous.
3. Increasing stress will reduce the fracture permeability. Since the effective roughness and tortuosity also increase, the Cubic Law cannot fully predict the permeability change. From the perspective of Modified Cubic Law, the mean aperture decrease will reduce the mechanical aperture e , and the increasing variance will increase the friction factor. Both effects cause the fracture permeability to decrease.
4. Capillary pressure in rock fractures is stress-dependent. The plateau area of the capillary pressure curve grows steeper with stress and entry pressure will increase. The mean aperture will affect the entry pressure. The variance of aperture distribution will affect both pore size distribution and entry pressure. The capillary behavior changes from more fracture-like to more porous media-like with increasing stress.
5. Limitations of this paper include local heterogeneity by grain distributions (Konzuk and Kueper, 2004);, simplification of pore occupancy model (Yang et al., 2013);. Further experiments and simulations are needed for better understanding of stress-dependent permeability and capillary pressure.

Acknowledgements:

The authors are grateful to ENI for their financial support to this research.

References:

- Abass, H. H., Khan, M. R. and Sierra, L. 2009, Understanding Stress Sensitive Tight Gas Reservoirs, *Saudi Aramco Journal of Technology*, summer, p11–21
- Babadagli, T. 2003, Evaluation of EOR Methods for Heavy-Oil Recovery in Naturally Fractured Reservoirs, *J. of Petroleum Science and Eng.*, vol. 37, no.1–2, Feb., 25–37
- Boussinesq, J. 1868, Mémoire sur l'influence des frottements dans les mouvements réguliers des fluides. (Study of the effect of friction on the laminar flow of fluids.); *Journal de Mathématiques Pures et Appliquées*, 2e série, tome 13, pp. 377–424

- Brace, W. F. 1978, A note on permeability change in geologic materials due to stress, *Pure Appl. Geophys.*, **116**, 627–633
- Brooks, R.H. and Corey, A.T. 1964. Hydraulic Properties of Porous Media. Hydrology Papers, No. 3, Colorado State U., Fort Collins, Colorado
- Cho, Y., Apaydin, O. G., and Ozkan, E. 2012, Pressure-Dependent Natural-Fracture Permeability in Shale and its Effect on Shale-Gas Well Production, presented at the SPE Annual Technical Conference and Exhibition held in San Antonio, Texas, USA
- Cook, A.M., Myer, L.R., Cook, G.W., and Doyle, F.M. 1990, The effect of tortuosity on flow through a natural fracture, Proceedings of the 31st US Symposium on Rock Mechanics, pp371–378
- de la Porte, J.J., Kossack, C.A. and Zimmerman, R.W. 2005, The effect of fracture relative permeability and capillary pressure on the numerical simulation of naturally fractured reservoirs, SPE ATCE, Dallas, TX, USA, October 9–12
- Esaki, T., Du, S., Mitani, Y., Ikusada, K., and Jing, L. 1999, Development of a shear-flow test apparatus and determination of coupled properties for a single rock joint. *Int. J. Rock Mech. Min. Sci.* **36**, 641–650
- Esaki, T., Du, S., Jiang, Y., Wada, Y. and Mitani, Y. 1998, Relation between mechanical and hydraulic apertures during shear-flow coupling test. Proc., 10th Japan Symp. Rock Mech., 91–96
- Gentier, S. 1986, Morphologie et comportement hydromécanique d'une fracture naturelle dans un granite sous contrainte normale; doctoral thesis, Univ. d'Orléans, France
- Huo, D and Benson, S.M. 2014, An Experimental Investigation of Stress-dependent Permeability and Permeability Hysteresis Behavior in Rock Fractures, AGU monograph Dynamics of Fluids and Transport in Fractured-Porous Media, submitted
- Huo, D and Gong, B. 2010, Discrete Modeling and Simulation on Potential Leakage through Fractures in CO₂ Sequestration, presented at SPE Annual Technical Conference and Exhibition, 19–22 September, Florence, Italy
- Johns, R. A., Steude, J. S., Castanier, L. M. and Roberts, P. V. 1993, Nondestructive measurements of fracture aperture in crystalline rock cores using X ray computed tomography, *Journal of Geophysical Research*, **98**(B2);, 1889–1900
- Karpyn, Z.T., Alajmi, A., Radaelli, F., Halleck, P.M., and Grader, A.S. 2009, X-ray CT and hydraulic evidence for a relationship between fracture conductivity and adjacent matrix porosity, *Engineering Geology*, **103**, 139–145
- Keller, A. A. 1997, High resolution CAT imaging of fractures in consolidated materials, *International Journal of Rock Mechanics and Mining Science*, **34**(3/4);, 358–371
- Lenormand, R., Zarcone, C., and Sarr, A. 1983, Mechanisms of displacements of one fluid by another in a network of capillary ducts, *J. Fluid. Mech.*, **16**, 3365–3376
- Liu, H., Wei, M., and Rutqvist, J. 2013, Normal-stress dependence of fracture hydraulic properties including two-phase flow properties. *Hydrogeol J.*, **21**: 371–382
- Muralidharan, V., Chakravarthy, D., Putra, E., and Schechter, D. S. 2004, Investigating Fracture Aperture Distributions under Various Stress Conditions Using X-Ray CT Scanner, presented at the Petroleum Society's 5th Canadian International Petroleum Conference (55th Annual Technical Meeting);, Calgary, Alberta, Canada, June 8 – 10
- Murata, S. and Saito, T. 2003, "Estimation of tortuosity of fluid flow through a single fracture." *Journal of Canadian Petroleum Technology*, **42**, 39–45
- National Research Council 1996, *Rock fractures and fluid flow: contemporary understanding and applications*, Washington, DC: The National Academies Press
- Patir, N. and Cheng, H.S. 1978, An average flow model for determining effects of three-dimensional roughness on partial hydrodynamic lubrication, *Journal of Lubrication Technology* **100**, 12–17

- Pini R., Krevor, S.C.M. and Benson, S.M. 2012, Capillary pressure and heterogeneity for the CO₂/water system in sandstone rocks at reservoir conditions, *Advances in Water Resources*, **38**, 48–59
- Pinzon, C., Chen, H.Y. and Teufel, L.W. 2000, Complexity of Well Testing Analysis of Naturally Fractured Gas Condensate Wells in Columbia, SPE 59013, presented at the 2000 SPE International Conference, Villahermosa, Mexico
- Pruess, K., and Tsang, Y. W. 1990, On two-phase relative permeability and capillary pressure of rough-walled rock fractures, *Water Resour. Res.*, **26**(9);, 1915–1926
- Pruess K. 2008, On CO₂ fluid flow and heat transfer behavior in the subsurface, following leakage from a geologic storage reservoir, *Environmental Geology*, June 2008, Volume **54**, Issue 8, pp 1677–1686
- Pyrak-Nolte, L.J., Cook, N.G. and Myer, L.R. 1990, Stratified percolation model for saturated and unsaturated flow through natural fractures, Proceedings of First Annual International High-Level Radioactive Waste Management Conference, vol. **1**. pp 551–558
- Raven, K.G., and Gale, J.E. 1985, Water flow in a natural rock fracture as a function of stress and sample size. *Int J Rock Mech Min Sci Geomech Abstr* **22**(4);:251–261
- Reitsma, S. and Kueper, B. H. 1994, Laboratory measurement of capillary pressure-saturation relationships in a rock fracture, *Water Resour. Res.*, **30**(4);, 865–878, doi:10.1029/93WR03451
- Renshaw, C.E. 1995, On the relationship between mechanical and hydraulic apertures in rough-walled fractures. *J. Geophys Res* **100**:24629–24636
- Tsang, Y. W. and Tsang, C. F. 1990, Hydrological Characterization of Variable-Aperture Fractures; *Rock Joints*, Barton & Stephansson (eds);, Balkema, Rotterdam
- Van Geet, M. and Swennen, R. 2001, Quantitative 3D-fracture analysis by means of microfocus X-ray computer tomography (μ CT);: an example from coal, *Geophysical Research Letters*, **28**(17);, 3333–3336
- van Genuchten MTh. 1980. “A closed form equation for predicting the hydraulic conductivity of unsaturated soils.” *Soil Sci. Soc. Am. J.* **44**:892–898
- Walsh, J. B. 1981, Effect of pore pressure and confining pressure on fracture permeability, *Int. J. Rock Mech. Sci. Geomech*, Vol. **18**, pp 429–435
- Walsh, R., McDermott, C., Kolditz, O. 2008, Numerical modeling of stress-permeability coupling in rough fractures. *Hydrogeol J* **16**:613–627
- Wan, T., Sheng, J. J. and Soliman, M. Y. 2013, Study Evaluates EOR Potential In Naturally Fractured Shale Reservoirs, December 2013 Exclusive Story, the American Oil and Gas Reporter
- Wang, F. P., and Reed, R.M. 2009, Pore Networks and Fluid Flow in Gas Shales, SPE-124253-MS, SPE Annual Technical Conference and Exhibition, 4–7 October, New Orleans, Louisiana
- Witherspoon, P.A., Wang, J.S.Y., Iwai, K., and Gale, J.E. 1980, Validity of cubic law for fluid-flow in a deformable rock fracture, *Water Resour. Res.*, **16**:1016–1024
- Yang, Z., Niemi, A., Fagerlund, F., and Illangasekare, T. 2013, Two-phase flow in rough-walled fractures: Comparison of continuum and invasion-percolation models, *Water Resour. Res.*, **49**, doi: 10.1002/wrcr.20111
- Zimmerman, R. W., Chen, D. W. and Cook, N. G. W. 1992, The effect of contact area on the permeability of fractures, *J. Hydrol.* **139**, 79–96